Wind Energy

WIND ENERGY
Wind Energ. 2016; **19**:1135–1150
Published online 14 August 2015 in Wiley Online Library (wileyonlinelibrary.com). DOI: 10.1002/we.1891

RESEARCH ARTICLE

Analysis of axial-induction-based wind plant control using an engineering and a high-order wind plant model

Jennifer Annoni[1], Pieter M. O. Gebraad[2], Andrew K. Scholbrock[2], Paul A. Fleming[2] and Jan-Willem van Wingerden[3]

[1] Department of Aerospace Engineering and Mechanics, University of Minnesota, Minneapolis, Minnesota, USA
[2] National Renewable Energy Laboratory, Golden, Colorado, USA
[3] Delft Center for Systems and Control, Delft University of Technology, Delft, The Netherlands

ABSTRACT

Wind turbines are typically operated to maximize their performance without considering the impact of wake effects on nearby turbines. Wind plant control concepts aim to increase overall wind plant performance by coordinating the operation of the turbines. This paper focuses on axial-induction-based wind plant control techniques, in which the generator torque or blade pitch degrees of freedom of the wind turbines are adjusted. The paper addresses discrepancies between a high-order wind plant model and an engineering wind plant model. Changes in the engineering model are proposed to better capture the effects of axial-induction-based control shown in the high-order model. Copyright © 2015 John Wiley & Sons, Ltd.

KEYWORDS
wind plant control; wind turbine control; wind turbine wakes

Correspondence
Jennifer Annoni, University of Minnesota, 110 Union St. SE, Minneapolis, Minnesota 55455, USA.
E-mail: anno0010@umn.edu

Received 3 September 2014; Revised 22 June 2015; Accepted 13 July 2015

1. INTRODUCTION

Grouping wind turbines in wind plants helps to reduce land use and costs of grid connection, installation, and maintenance; however, when wind turbines are placed relatively close to each other, some of the turbines will impact the performance of downstream turbines that are in the path of their wake. Applying plant-wide controls to coordinate the operation of the turbines and mitigate this effect is a topic of increasing interest.

Various wind plant control strategies have been proposed in existing literature. In one of the methods, the wakes are redirected away from downstream turbines through misalignment of the rotor from the freestream direction using yaw actuation.[1–6] Other proposed methods alter the operation of either the pitch or torque controller to reduce the axial induction of an upstream turbine to allow higher velocity wind to reach a downstream turbine and increase overall power capture. These methods are classified as 'axial-induction-based control'.

Several simulation studies investigate the effect of axial-induction-based control on power production. The studies use wake models that range from engineering models[7–11] to more high-fidelity computational fluid dynamics (CFD) simulators[12–15] to find the optimal settings of axial induction for various wind plants. Not all studies report a beneficial effect. For example, the wind plant large eddy simulation (LES) study by Nilsson *et al.*[16] tested axial-induction-based control using a range of pitch offsets, but an increase of the total power was not achieved. In addition to simulation studies, wind-tunnel experiments of axial-induction-based controls have been performed with scaled turbines. In the two-turbine tests by Adaramola and Krogstad,[2] the results showed an increase in total power production of turbine rows when reducing the power extraction of the front turbines using pitch control. Finally, experimental data from wind plants with full-scale industrial wind turbines is scarce.[17] A relevant study is from Boorsma,[18] which reported a systematic power production increase for the first two in a row of 2.5-MW turbines with 3.8 rotor diameter spacing when applying axial-induction-based control via a pitch offset on the front turbine.

In general, a wide range of production increases through axial-induction-based control have been reported,[17] including cases in which no increase was found. In our studies, we have noticed similar discrepancies when using different models. In

this paper, we present our studies on axial-induction-based control, performed using both an engineering and a high-order CFD model for several basic layouts for wind plants. The two models considered in this paper are the FLOw Redirection and Induction in Steady-State (FLORIS) engineering model and the Simulator fOr Wind Farm Applications (SOWFA), a high-fidelity CFD simulation tool. We analyze the results of each, consider apparent discrepancies between the models and propose methods to resolve the differences between FLORIS and SOWFA based on physical considerations. Note that this paper does not go into detail about finding an optimal setting for a wind plant given a specific layout; rather, this paper extends an existing control-oriented model to provide an engineering model that is suitable for the design and analysis of axial-induction-based wind plant control strategies.

Section 2 of this paper provides a detailed description of the investigated axial-induction-based control strategy. Section 3 provides details about the FLORIS model and SOWFA. Section 4 provides an overview of the simulation setups used. Section 5 presents the model-based analyses of the axial-induction-based control concept with SOWFA and FLORIS and notes the discrepancies between the models. Section 6 proposes and evaluates additions to the engineering model to better fit the high-order model results. Conclusions and suggestions for future work are provided in Section 7.

2. AXIAL-INDUCTION-BASED CONTROL BACKGROUND

In the control strategy studied in this paper, the power extraction of the upstream turbines is adjusted to influence the velocity deficits in the wakes. This method is referred to as axial-induction-based control, because the control settings are adjusted to influence the axial-induction factor of the turbine. The axial-induction factor, a, is the fractional decrease in wind velocity between the freestream and the turbine rotor (Figure 1). The collective blade pitch angle and generator torque, which are standard inputs on a utility-scale turbine, can be used to adjust the axial induction. In the wake behind the rotor, the flow expands and recovers to the freestream conditions farther downstream because of the momentum transfer at the edges of the wake (also shown in Figure 1). Downstream turbines that are in the path of wakes of upstream turbines experience reduced wind speeds in the wake. This results in lower power production on those downstream turbines. The wake effects cause a coupling between the control settings on upstream turbines and the power production on downstream turbines.

The amount of total power production gain that can be achieved by axial-induction-based control is dependent on the aerodynamic characteristics of the turbine and on the atmospheric conditions. Important characteristics of the turbine are the power coefficient, C_P, and the thrust coefficient, C_T, which both are dependent on the tip-speed ratio (TSR) and the pitch of the blades, β.[19] The TSR is given by

$$\lambda = \frac{\omega R}{U} \tag{1}$$

where R is the rotor radius, ω is the rotor speed and U is the freestream velocity. The rotor speed, and thus the TSR, can be influenced by adjusting the generator torque or changing the lift forces on the rotor blades by adjusting the blade pitch. The C_P determines the efficiency of the rotor in extracting power from the wind. The steady-state power extraction of the rotor, P, is given by

$$P = \frac{1}{2}\rho A C_P(\beta, \lambda) U^3 \tag{2}$$

where A is the area swept by the rotor and ρ is the air density. The C_T determines the rotor's thrust force on the flow, F_T, given by

$$F_T = \frac{1}{2}\rho A C_T(\beta, \lambda) U^2 \tag{3}$$

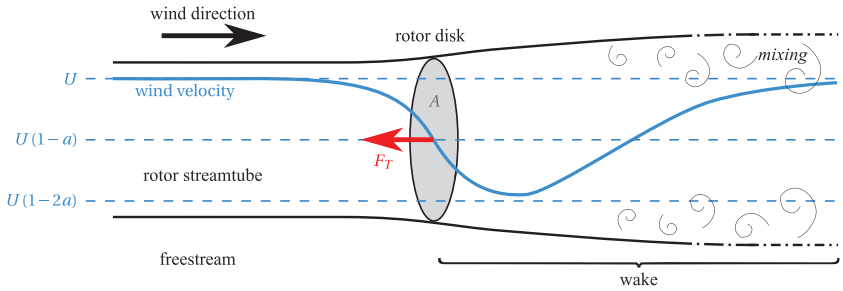

Figure 1. Simplified representation of the wake and upstream induction zone of the wind turbine rotor. The blue solid line represents a possible time-averaged velocity profile over the wake centerline.

Wind Energ. 2016; **19**:1135–1150 © 2015 John Wiley & Sons, Ltd.
DOI: 10.1002/we

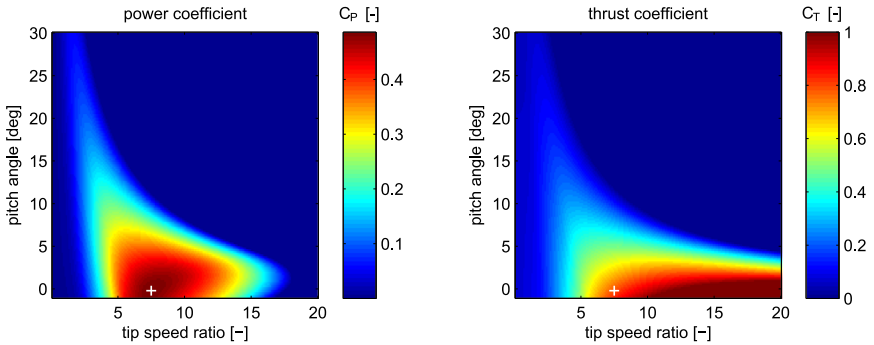

Figure 2. Power and thrust coefficient of the NREL 5-MW turbine[20] as a function of blade pitch and TSR. In both surfaces, the cross (+) indicates the maximum-C_P operation point.

The thrust of the rotor determines the reduction of velocity over the rotor plane—i.e., the axial induction, a. It follows from actuator disk momentum theory that if it is assumed that there is no recovery of the wake, the extraction of energy over the rotor reduces the velocity in the wake behind the turbine to

$$U_{\text{wake,min}} = U\,(1 - 2a) \tag{4}$$

where the axial-induction factor, a, can be related to the thrust factor by

$$a = \frac{1}{2}\left(1 - \sqrt{1 - C_T}\right) \tag{5}$$

In reality, there is wake recovery through convection and diffusion of momentum; therefore, $U_{\text{wake,min}}$ can be considered a lower bound on the wind velocity in the wake.

In below-rated wind conditions, the axial-induction-based control concept relies on the fact that at the maximum operating point of a single turbine, the power production sensitivity to the control settings is small—typically, the C_P-surface is flat around its optimal pitch angle and TSR, whereas the thrust factor, C_T, is more sensitive to the pitch and TSR around that operating point, as shown in Figure 2. Therefore, when deviating a small amount from the point of maximum C_P of the upstream turbines, the power production of that turbine will reduce only a small amount, whereas the axial induction will reduce enough to significantly increase the velocity in the wake. Thus, the ratio of the gradients of the C_T and C_P surfaces around optimum operation determine how much the wake velocity can be increased by reducing the power production on the upstream turbine. Under the right circumstances, this increase in velocity downstream of the rotor will increase the power of the downstream turbine more than the loss in power production on the upstream turbine.

In addition to rotor characteristics, many factors affect the amount of potential production increase from axial-induction-based control. This includes the amount of overlap between the wake and the downstream turbines. If the overlap is small, the relative gain is small. The overlap is determined by the wind direction, the expansion of the wake and the relative positions of the turbines. Also, the overlap changes over time because of wake meandering (oscillating movements of the wake caused by large-scale turbulence[21,22] and/or rotor vortex shedding[23]). Additionally, ambient atmospheric turbulence intensity, determined by inflow turbulence and the atmospheric thermal stability conditions, influences wake recovery.[24,25] With more ambient turbulence, the wake velocity recovers to the surrounding flow velocity in a shorter distance, because there is more mixing, which results in lower power gains when using axial-induction-based control.

3. MODELS

In wind plant controls, computationally efficient engineering models of wind plant wake effects are useful to quickly find optimized control settings using iterative algorithms, whereas high-fidelity wind plant models may be used for validation. In this section, we discuss the engineering and the high-fidelity model that are used in Section 5 to study the axial-induction-based control concept.

3.1. Engineering model: FLORIS

The FLORIS model (developed by Gebraad *et al.*[6]) is a combination of Jensen's model,[26,27] a model for wake deflection through yaw[3] and further modifications to better model the wake velocity profile and effects of partial wake overlap. The simulations analyzed in this paper incorporate turbine scenarios with fully overlapping wakes, which result in the FLORIS

model behaving in a way that is similar to the Jensen model. The FLORIS model captures characteristics achieved by SOWFA in yaw-based wake redirection control simulations. In this paper, it is adopted for axial-induction-based control.

The steady-state power of each turbine i, denoted as P_i, is given by the FLORIS model as

$$P_i = \frac{1}{2}\rho A_i C_P\left(a_i\right) U_i^3 \tag{6}$$

where ρ is the air density, A_i is the area of the rotor, C_P is the power coefficient and U_i is the effective wind speed at the turbine i. The rotor axial-induction factor, a_i, has been related to C_P by actuator disk theory:[19]

$$C_P\left(a_i\right) = 4a_i\left(1-a_i\right)^2\eta \tag{7}$$

where η is a correction factor applied in the FLORIS model to account for losses. A value $\eta = 0.8051$ is used to match the maximum $C_P = 0.4771$ of the National Renewable Energy Laboratory (NREL) 5-MW turbine in SOWFA, assuming an idealized axial-induction factor of $a = \frac{1}{3}$.

The wake velocity profile in FLORIS incorporates three regions: the (inner) near-wake zone (indexed $q = 1$), the (middle) far-wake zone ($q = 2$) and the (outer) mixing zone ($q = 3$), instead of the single region in Jensen's model. The diameters of the wake zones of a turbine i, $D_{\mathrm{w},i,q}$, expand proportionally with downstream distance:

$$D_{\mathrm{w},i,q}\left(x\right) = \max\left(D_i + 2k_e m_{e,q}\left[x - X_i\right], 0\right) \text{ for } x > X_i \tag{8}$$

where D_i is the rotor diameter and $(x - X_i)$ is the downstream distance between the position of the turbine, X_i, and a downstream point, x. Coefficient k_e is a global wake expansion factor, and $m_{e,q}$ defines the relative expansion of the wake zones set as $m_{e,1} = -0.5$, $m_{e,2} = 0.22$ and $m_{e,3} = 1$, such that the near-wake zone contracts over distance, and k_e defines the expansion of the outer mixing zone. The effective velocity at a downstream turbine j is found by combining the effect of the wakes of the upstream turbines i, weighting the wake zones by their overlap with the rotor as

$$U_j = U_\infty\left(1 - 2\sqrt{\sum_i\left[a_i\sum_{q=1}^{3}c_{i,q}\left(X_j\right)\min\left(\frac{A_{i,j,q}^{\mathrm{overlap}}}{A_j}, 1\right)\right]^2}\right) \tag{9}$$

where U_∞ is the freestream velocity, $A_{i,j,q}^{\mathrm{overlap}}$ is the overlap area of a wake zone q of a turbine i with the rotor of turbine j and $c_{i,q}(x)$ is a coefficient that defines the recovery of a zone q to the freestream conditions:

$$c_{i,q}\left(x\right) = \left(\frac{D_i}{D_i + 2k_e m_{U,q}\left[x - X_i\right]}\right)^2 \tag{10}$$

where $m_{U,q}$ are scaling factors that ensure that the velocity in the outer zones of the wake will recover to the freestream conditions faster than in the inner zones. The parameters of the model were tuned to $m_{U,1} = 0.5$, $m_{U,1} = 1.5$, $m_{U,1} = 5.5$ and $k_e = 0.065$ to match the results from the SOWFA wake simulations. The most influential parameter is k_e, because it defines both wake expansion and recovery.

3.2. High-order model: SOWFA

The simulator for wind farm applications is a high-fidelity large-eddy simulation tool that was developed at NREL for wind plant studies. SOWFA is a CFD solver based on OpenFOAM (OpenCFD Ltd., Bracknell, UK) coupled with NREL's FAST wind turbine simulator.[28–30] SOWFA has been used in previous wind plant control studies (e.g., in the works of some authors[4–6]).

The simulator for wind farm applications uses an actuator line model coupled with FAST to study turbines in the atmospheric boundary layer. Specifically, SOWFA solves the three-dimensional incompressible Navier–Stokes equations and transport of potential temperature equations, which take into account the thermal buoyancy and earth rotation (Coriolis) effects in the atmosphere.

The simulator for wind farm applications calculates the unsteady flow field to compute the time-varying power, velocity deficits and loads at each turbine in a wind plant. This level of computation, with high-fidelity accuracy, takes in the order of days to run on a supercomputer using a few hundred to a few thousand processors, depending on the size of the wind plant. The simulations run for this study were performed on NREL's high-performance computer Peregrine.[31]

Wind Energ. 2016; **19**:1135–1150 © 2015 John Wiley & Sons, Ltd.
DOI: 10.1002/we

Studies have been performed to validate SOWFA. For example, SOWFA has been compared with the 48-turbine Lillgrund wind plant field data and shows good agreement through the first five turbines in a row aligned with the wind direction.[32] In addition, SOWFA has been tested to verify that it captures the inertial range in the turbulent energy spectra and the log-layer in the mean flow, both of which characterize a realistic atmospheric boundary layer.[30] Further validation studies are being conducted.

4. SIMULATION SCENARIOS

In Section 5, three scenarios are simulated to study the axial-induction-based control concept: a single-turbine scenario, a scenario with two turbines aligned in the flow spaced seven rotor diameters ($7D$) apart and a scenario with five aligned turbines with a $5D$ spacing. The simulated turbines are NREL 5-MW baseline turbines,[20] which have a rotor diameter $D = 126\,\text{;m}$. Details about the positioning of the turbines in the domain in each case are given in Figures 3 and 4. The spatial discretization mesh for CFD is refined in two steps in a rectangular region, with the smallest cells containing the turbine rotors, the axial-induction zones of the rotor, and a large part of the wake. Farther from the turbines, the mesh is coarser to reduce computation time.

In each case, the conditions simulated in SOWFA are based on the study reported by Churchfield *et al.*[30] They consist of a neutral atmospheric boundary layer with a low aerodynamic surface roughness value of 0.001 m, typical for offshore conditions. The generated inflow, coming from the southwest (300°), has a horizontally averaged wind speed of $8\,\text{m}\,\text{s}^{-}1$ and a turbulence intensity of 6% at the turbine hub height.

In the one-turbine and two-turbine simulations, we use a simulated time length of 1,000 s to let the wakes develop through the domain. In the five-turbine scenario, a simulated time length of 2,000 s was used.

The same scenarios are simulated in the FLORIS model by specifying the same turbine dimensions and spacing and the same freestream velocity. The wake parameters are set to match the recovery and expansion properties found in SOWFA based on the power levels of the turbines. This paper focuses on comparing FLORIS to SOWFA results for one atmospheric condition, with a range of control settings. Note that changes in the atmospheric conditions would change the wake properties, including the coupling of the control settings and the wake interaction.

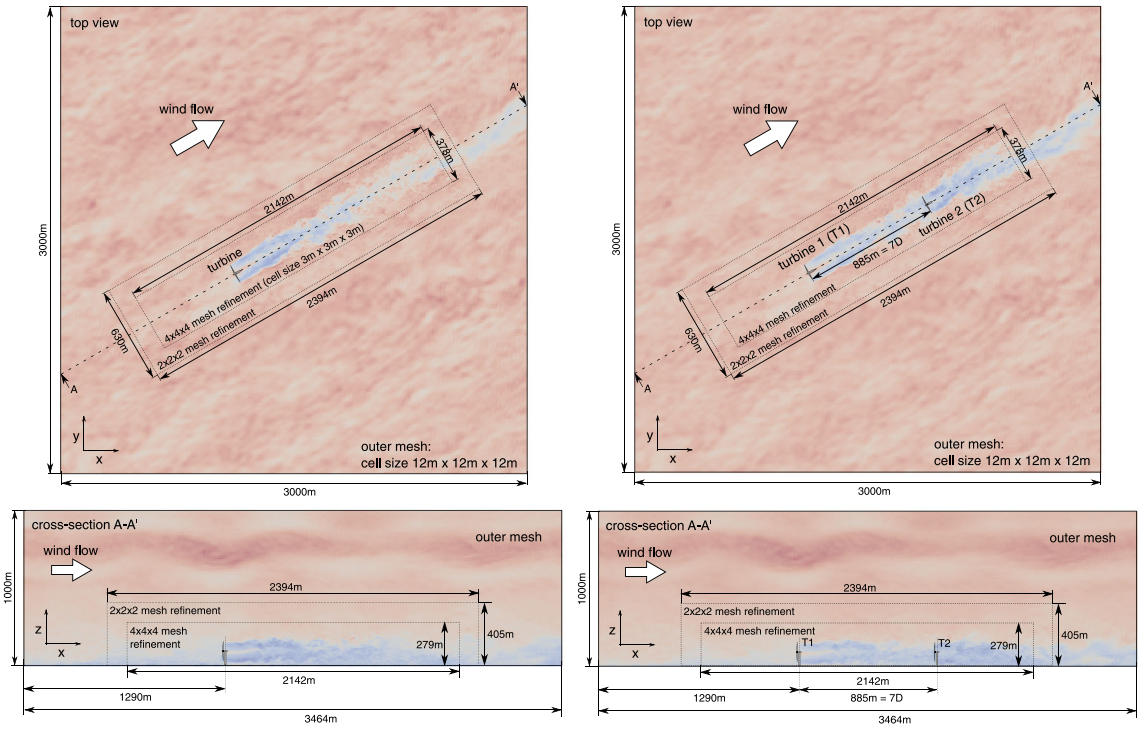

(a) Single-turbine case. **(b)** Two-turbine case.

Figure 3. Overview of (a) single-turbine and (b) two-turbine simulation setups in a domain of 3 km by 3 km (horizontal) by 1 km (height).

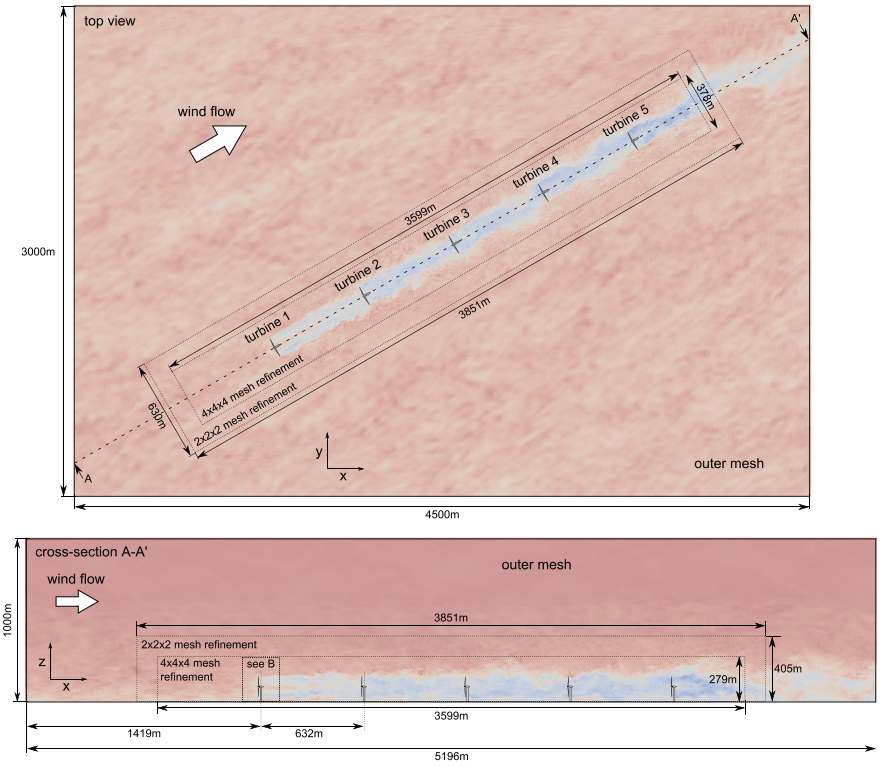

Figure 4. Setup of the five-turbine case in a domain of 3 km by 4.5 km (horizontal) by 1 km (height).

5. EVALUATION OF AXIAL-INDUCTION-BASED METHODS IN AN ENGINEERING AND HIGH-ORDER MODEL

This section evaluates the overall impact of axial-induction-based control for the two-turbine and five-turbine scenarios; first, with the engineering model, FLORIS, and then the results are compared with the simulation results of the high-order model, SOWFA. Discrepancies between the two models are described. Section 6 attempts to address these discrepancies.

5.1. Two-turbine scenario

5.1.1. Evaluation of axial-induction-based control strategies using FLORIS.

To analyze the effectiveness of axial-induction-based control in the two-turbine scenario using FLORIS, a range of operating points were considered. The axial-induction factor of the upstream turbine, a, was reduced by as much as 60% from the value of $a = 1/3$ that would yield maximum power for the individual turbine (baseline). Also, a range of expansion coefficients, k_e, were considered that varied from 0.005 to 0.125. A typical k_e value in the literature is 0.1 .[33] The value of the FLORIS model main parameter, k_e, was fitted to SOWFA data with a value $k_e = 0.065$. This coefficient can be thought of as the averaged effects of wake expansion and turbulence: a higher wake expansion coefficient, k_e, corresponds to faster wake expansion and a faster wake recovery through turbulent mixing. Figure 5 shows the results of using FLORIS to predict the effects axial-induction-based control for the two-turbine scenario. For all k_e values, there is an optimal setting for a two-turbine array that will increase the total power produced compared with the baseline case in which both turbines run at optimal C_P. Table I summarizes the optimal upstream turbine reduction in a and the resulting percentage of power gained compared with the baseline case for some k_e values.

The overall power that can be gained from axial-induction-based control decreases as the wake expansion coefficient increases. With a higher k_e, the wake expands more and recovers faster, and the energy sacrificed by the upstream turbine goes around the downstream turbine and is not captured by the downstream turbine. However, as previously stated, regardless of the choice of k_e, reducing the axial induction of the front turbine increases the total combined power output. This result agrees with studies in the literature in which the Jensen model was used to predict the effects of axial-induction-based control .[7–10]

Wind Energ. 2016; **19**:1135–1150 © 2015 John Wiley & Sons, Ltd.
DOI: 10.1002/we

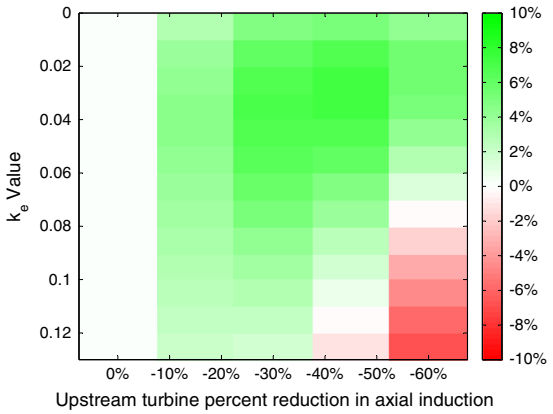

Figure 5. Baseline power gain with axial-induction-based control using the FLORIS model.

Table I. Summary of FLORIS-predicted axial-induction-based control results.

k_e	% Reduction of a	Overall % gain in power
0.025	45	7.23
0.065	30	5.74
0.125	15	1.97

5.1.2. Evaluation of axial-induction-based control strategies using SOWFA.

Given the results of the FLORIS model simulation, and similar results for Jensen model evaluations of axial-induction-based wind plant control shown in the literature, in this section, we investigate whether these results can be observed in the higher-order simulator SOWFA.

Figure 6(a) shows the results of a test of axial-induction-based wind plant control for the two-turbine setup. The axial induction is modified for the front turbine by offsetting the collective pitch angle from the optimum setting (zero pitch offset). The analysis shows that the turbine-level power optimal setting also yields maximum power production for the total wind plant. Although the effect of reduction of the front rotor axial induction causes an increase in power of the second turbine in the row, the power lost on the first turbine by offsetting the pitch is not regained at the second turbine. Figure 6(b) shows the results of reducing the axial induction of the front turbine by modifying the generator torque. A scaling factor, α, is applied on the regular below-rated rotor speed control law[20] of the front turbine, so that the applied generator torque is $T = \alpha * K * \omega^2$ with $K = 0.0179$ Nm/RPM^2, resulting in a deviation from the turbine-level optimal gain K for maximum power production.* Figure 2 and equation (5) show that a reduction in TSR is needed to decrease C_T and lower the rotor axial-induction factor. This is achieved by increasing the generator torque ($\alpha > 1$). Yet, the C_T has a low sensitivity to the TSR, and the possible increase of the generator torque is limited because the rotor may stall when a temporary reduction of wind speed occurs. When increasing torque on the upstream turbine, a small increase in power on the downstream turbine can be observed; however, as in the pitch case, there is not enough power increase on the downstream turbine to compensate for the power production loss on the front turbine from adjusting the torque, and a decrease in total power production results.

To understand these results, an investigation was performed using the single-turbine setup. In this simulation analysis, we compared a two-degree pitch offset on the turbine to the baseline case. For both simulations, we extracted flow data at planes perpendicular to the mean wind direction at several distances downstream of the rotor. The kinetic power density of the flow through the slice is calculated as

$$P_{\text{density}} = u_{\text{axial}} \left(\frac{1}{2} \rho \vec{U} \vec{U}^T \right) \tag{11}$$

where u_{axial} is the axial component of the velocity of the flow through a slice and $\vec{U}$ is the velocity vector. By subtracting the kinetic power density of the slices for the baseline case from those of the offset case, the kinetic power added to

*We found that in the SOWFA simulations, the generator torque gain yielding optimal TSR for maximum power production, K, is different from the optimal value $K = 0.0256\ Nm/\text{RPM}^2$ in the Aerodyn simulations reported in the work of Jonkman *et al.*[20]

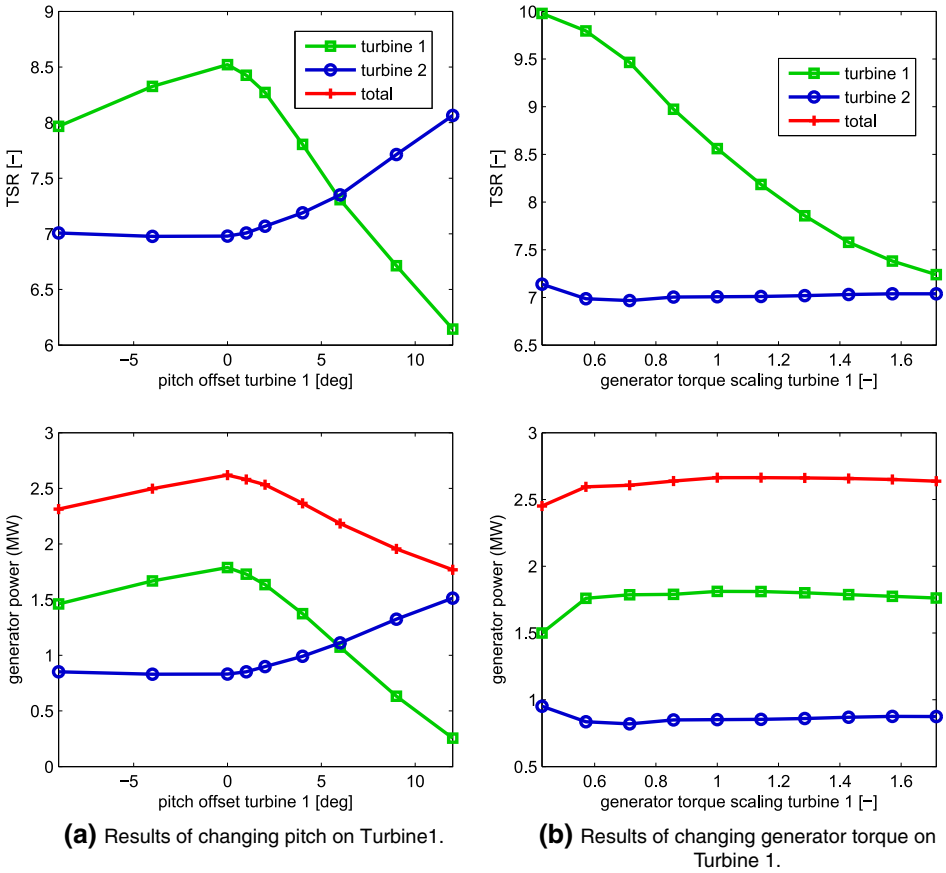

(a) Results of changing pitch on Turbine1. **(b)** Results of changing generator torque on Turbine 1.

Figure 6. SOWFA simulation results of using the axial-induction control concepts on a two-turbine setup, using pitch (left) or generator torque (right) offsets on the front turbine (1) to affect the power on the downstream turbine (2).

the wake by pitching the turbine is calculated. Figure 7(a) shows the difference in the kinetic power density of the wind flowing through the cut-through slices. By visualizing the rotor plane of a 'virtual' rotor of equal size placed downstream aligned in the wind direction, Figure 7(a) shows that the kinetic power conserved in the flow by using a pitch angle offset on the turbine is mostly going outside of the downstream rotor plane, because the wake expands and meanders outside of the rotor area; therefore, the pitch offset on the front turbine would cause a production loss on the two-turbine setup, as it results in accelerating the flow surrounding the downstream rotor rather than increasing the downstream turbineâĂŹs power production. A larger portion of the energy is lost when the downstream turbine is placed farther downstream. (Note that $6D$ to $8D$ are common distances in real wind plants.) A second cause for the limited ability to improve production at the downstream turbine through pitch control offsets on the upstream turbine is that a reduction in turbine thrust force can reduce turbulence in the wake and thereby the wake recovery, which has a negative effect on the velocity at the downstream turbine.

Based on the results shown in Figure 7(a), an energy balance was made, which is shown in Figure 7(b). The balance predicts the effect of the front turbine's pitch offset on the power of a downstream turbine placed at a range of distances. In the balance, ΔP_{wind} represents the total wind kinetic power increase in the area of a virtual downstream rotor. This power increase is compared with the power lost on the upstream turbine by pitching, denoted by ΔP_{T1}. The comparison is made for a range of distances of the virtual downstream rotor. Each of the power differences is normalized to the baseline power of the upstream turbine, $P_{\text{T1, baseline}}$. If we consider that the NREL 5-MW turbine can operate at a maximum $C_{P,\max} = 0.48$ efficiency,[20] it follows that the maximum energy gain on a downstream turbine is $C_{P,\max}\Delta P_{\text{T1}}$. Then, the balance predicts that with the simulated turbine and flow conditions, it is impossible to recover the energy lost through offsetting the pitch on the upstream turbine, because $C_{P,\max}\Delta P_{\text{wind}} < \Delta P_{\text{T1}}$. Thus, it predicts that an increase in total power cannot be achieved with the tested pitch offset when the downstream turbine is placed at a realistic spacing (more than $1D$).

Reviewing these results, SOWFA shows that for this simulation setup there is no axial-induction reduction setting for the front turbine that increases the total power compared with the baseline case in which the front turbine maximizes its

Wind Energ. 2016; **19**:1135–1150 © 2015 John Wiley & Sons, Ltd.
DOI: 10.1002/we

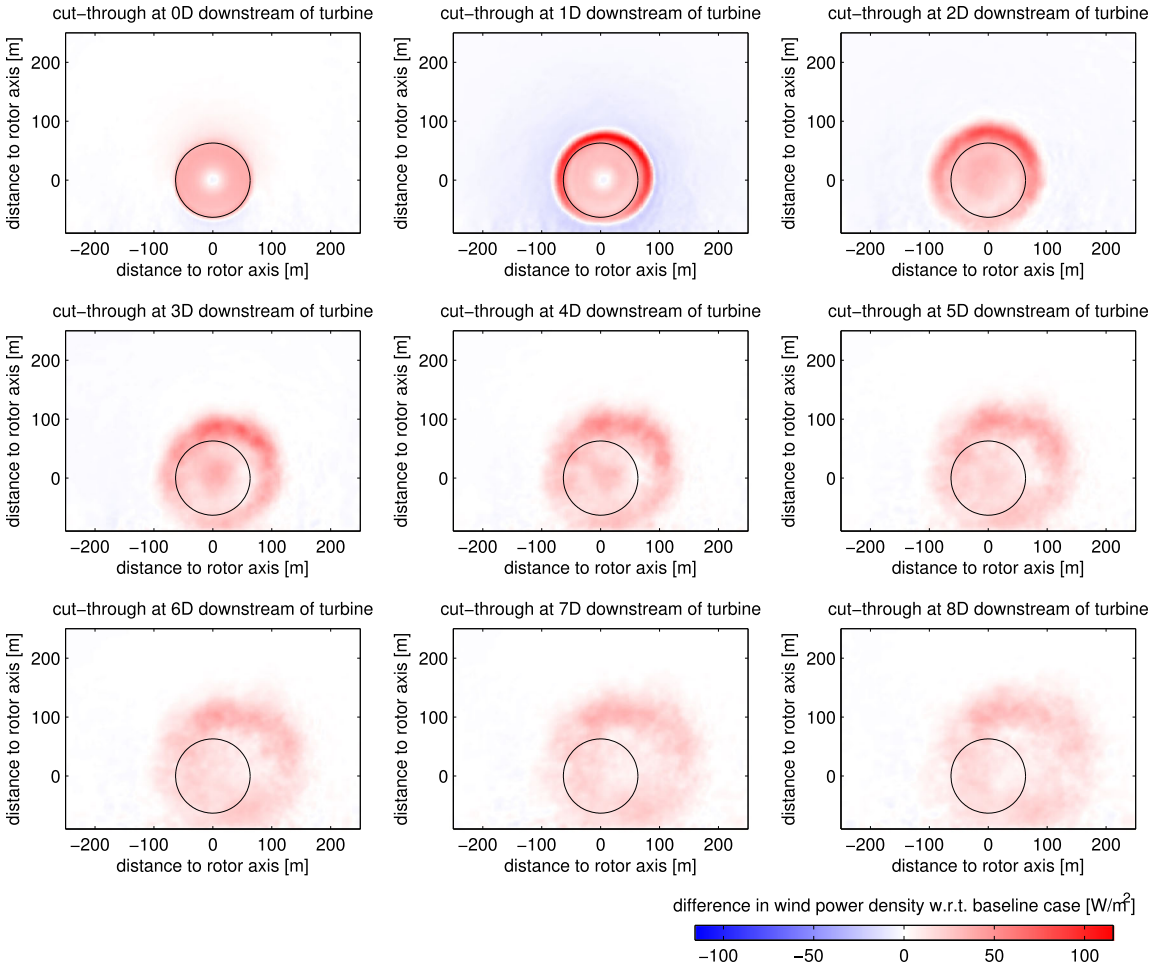

(a) Kinetic power added to the flow behind the turbine by introducing a 2° pitch offset. The black circle visualizes the location of a second turbine rotor.

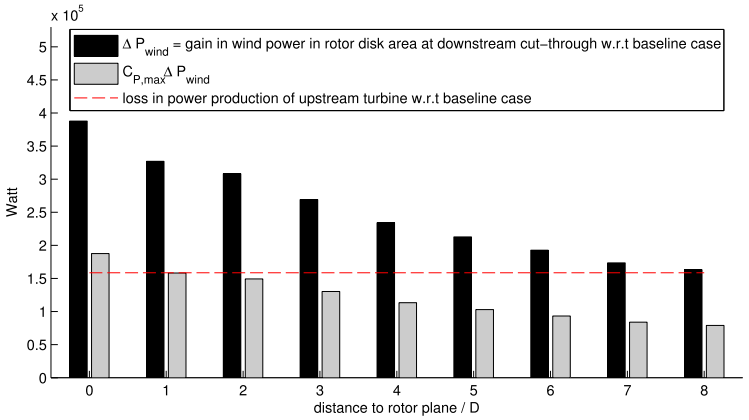

(b) Energy balance based on the results shown in Figure 7a: power lost on the upstream turbine by introducing a 2° pitch offset, ΔP_{T1} (red line), compared to flow power added in a virtual downstream rotor plane, ΔP_{wind} (black bar), and the maximum power that can be recovered by a downstream turbine, $C_{P,\max}\Delta P_{\mathrm{wind}}$ (gray bar).

Figure 7. Power balance for the wake of a single turbine with a 2° offset.

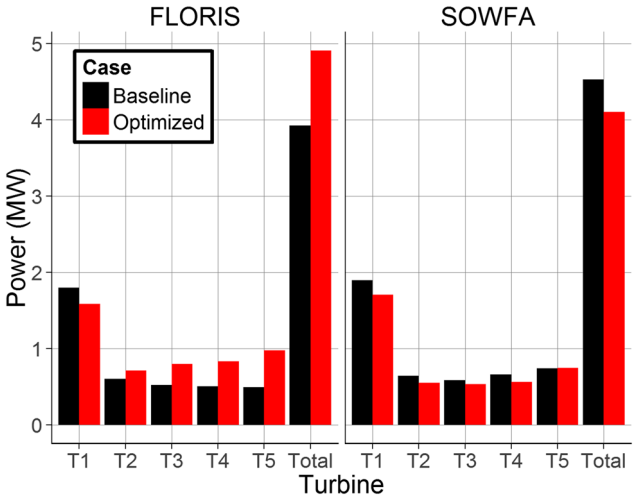

Figure 8. Results of the five-turbine simulations using FLORIS and SOWFA.

own power. Note that the simulated conditions, which have a relatively low turbulence and alignment of the turbine row with the wind direction, yield large wake losses; therefore, they represent a nearly ideal case for axial-induction-based control given the characteristics of the turbines, and it is not expected that the potential will improve significantly for other realistic conditions.

The SOWFA results for this case are in direct conflict with previous results based on the FLORIS model: Figure 5 suggests that with $k_e = 0.065$ (the value corresponding to this SOWFA simulation), a wide range of axial-induction reduction amounts should yield a total power improvement.

5.2. Five-turbine scenario

In addition to the two-turbine study, a similar study was performed with five turbines using both FLORIS and SOWFA. Two cases were simulated per model, one in which the turbines were each operating at their turbine-level optimal axial-induction factor $a = 1/3$ (baseline) and one in which the turbine axial-induction factors were optimized for maximum total production of the setup using the Jensen model. In the optimized case, the optimal turbine axial-induction factors were found by a grid search over the range of possible values.

To recreate the same cases in SOWFA, the turbine axial-induction settings used in FLORIS were converted to pitch values in SOWFA. This was obtained by computing the C_P value from the axial-induction factor using equation (7). The pitch was found from the C_P value by using a lookup table based on the upstream turbine power data shown in Figure 6(a).

The FLORIS and SOWFA simulation results are shown in Figure 8. As in the two-turbine case, FLORIS predicted a substantial total power increase, whereas the SOWFA simulations yielded a noticeable decrease. Comparing individual turbine power outputs further illustrates the discrepancy between the models. FLORIS indicated that derating the upstream turbines will result in power increases at each of the downstream turbines. Using the same operating points in SOWFA, there were significant losses at each turbine, with the exception of a small gain on the last turbine. Section 6 considers the source of these discrepancies and proposes modifications to resolve them.

6. MODIFICATIONS TO THE ENGINEERING MODEL

Section 5 showed that there are important differences in the power output predictions of the engineering model, FLORIS, and the high-order model, SOWFA, when simulating axial-induction-based control. This discrepancy is in line with the literature record discussed in Section 1.

As noted before, in these cases with full wake overlap, the Jensen model and its extension, FLORIS, behave similarly in that the wake properties are primarily defined by the wake expansion coefficient. The differences in the simulation results using SOWFA for cases when the upstream turbine is derated suggests that changes in axial induction are a particular non-modeled element of the Jensen-type models. This section presents an extension to FLORIS that applies more generally to other Jensen-type models to better model the wake behavior when axial-induction-based control is applied.

Wind Energ. 2016; **19**:1135–1150 © 2015 John Wiley & Sons, Ltd.
DOI: 10.1002/we

We return to the FLORIS and SOWFA two-turbine simulations in which the pitch angle is progressively increased (Figure 6(a)). Increasing the pitch angle seemed to be the most hopeful approach to implement axial-induction-based control, based on the results in Figure 6. Figure 9 shows a comparison of the power predicted for the upstream and downstream turbines by FLORIS and SOWFA for a range of upstream turbine pitch angles.

Figure 9 shows that although the FLORIS model with the originally fitted k_e of 0.065 is a good fit for the first turbine, it fits the second turbine only for the baseline axial-induction setting for the upstream turbine. The primary parameter for tuning the FLORIS model is k_e, the wake expansion and recovery rate.

First, we investigated whether there is a better selection for k_e than the originally fitted one of 0.065. Figure 9 shows comparisons between SOWFA and FLORIS for several different k_e values. Figure 9(b) shows that no single value of k_e is a good fit for the range of axial-induction settings of the upstream turbine.

6.1. FLORIS-vk$_e$: adjusting wake expansion and recovery to axial induction

Based on the results discussed in the previous section, a possible solution to the discrepancy would be to allow k_e to vary with the axial-induction setting of the upstream turbine. As described earlier, k_e characterizes the wake expansion and recovery, and it is reasonable that the amount of induction impacts this process.

To investigate this possibility, for each axial-induction setting, the value of k_e was determined that would provide the best agreement between the FLORIS model and SOWFA, and the results are shown in Figure 10. There appears to be a linear relationship between k_e and axial induction; therefore, a modification to the FLORIS model is proposed in which k_e is not fixed but is computed from the upstream turbine axial induction, a. For this scenario, the best fit is

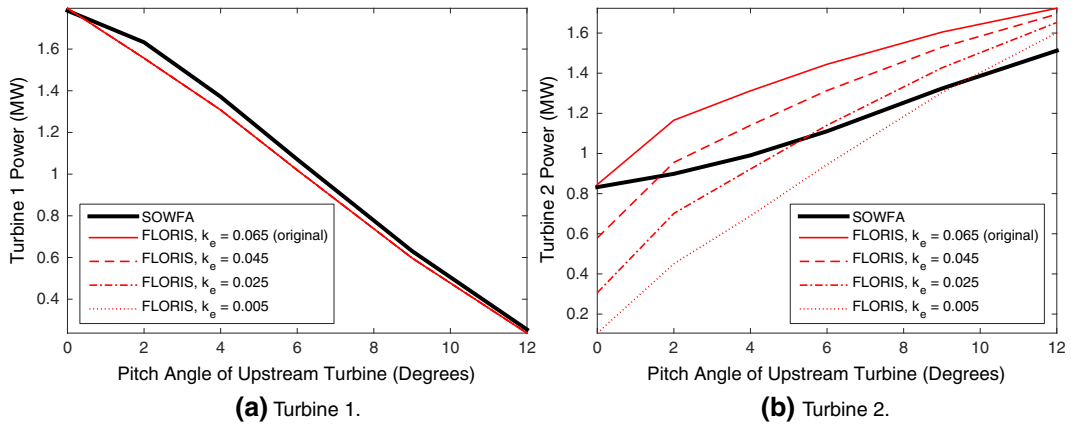

Figure 9. A comparison of FLORIS to the SOWFA results for the two-turbine scenario using different values for k_e.

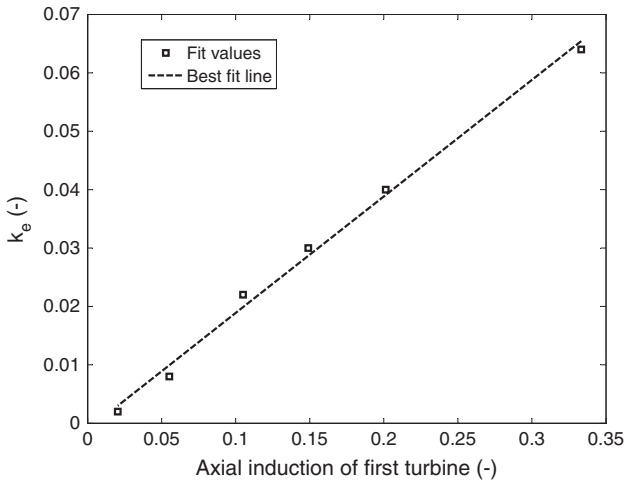

Figure 10. Linear fit between k_e and the front turbine axial induction.

$$k_e = m * a + b \tag{12}$$

where m and b are fit to the SOWFA cases with an R^2 value of 99.5%, with $m = 0.1995$ and $b = -0.0011$. In this linear relationship, as a decreases, k_e also decreases, explaining in part the apparent inability for axial-induction-based control to increase overall power in SOWFA. Table II shows that this effect counteracts the increase in near-wake velocity because of a reduction in axial induction. As described in Section 2, decreasing the axial-induction factor will decrease the velocity deficit behind the turbine as well as the thrust force that the turbine exerts on the flow. This impacts the wake expansion and turbulence in the flow. When decreasing the axial induction, the induced wake expansion and recovery rate, defined in FLORIS as k_e, will decrease. Because of a decrease in wake recovery, the downstream turbine will see a similar velocity whether the upstream turbine is operating at the turbine-level optimal axial-induction factor, $a = \frac{1}{3}$, or whether the upstream turbine is derated.

The FLORIS model was modified to include the variation in k_e given in equation (12). This modified FLORIS model is referred to as FLORIS-vk$_e$. Figure 11 shows the results from comparing the SOWFA, FLORIS and FLORIS-vk$_e$ predictions for the two-turbine case. FLORIS-vk$_e$ yielded a substantial improvement in modeling the impact of decreasing the axial induction of the upstream turbine. Additionally, the ability to increase total power, evident in the FLORIS model, has now been removed, which is in line with the SOWFA results. Next, the FLORIS-vk$_e$ model is reanalyzed for the five-turbine scenario.

6.2. FLORIS-vk$_e$3: adjusting wake expansion and recovery to wake overlap

For the five-turbine scenario, two cases were considered that were modeled using both FLORIS and SOWFA. These cases included a baseline case in which the turbines operated at turbine-level optimal induction, and a case in which some turbines were derated to yield an optimal result in the Jensen model. For each case, Figure 12 compares the FLORIS-vk$_e$ predictions to those of FLORIS and SOWFA.

Figure 12(a) shows that FLORIS and FLORIS-vk$_e$ yielded equivalent predictions for the baseline case because in that case each turbine operates at its baseline axial induction, which resulted in the same k_e value. The optimized case (Figure 12(b)) showed a substantial reduction from the FLORIS to the FLORIS-vk$_e$ model, which better agreed with SOWFA. This is further underlined in Figure 12(c), which shows the percent change in power from the baseline to optimized case.

However, focusing on the baseline case, Figure 12(a) indicates that both the FLORIS and FLORIS-vk$_e$ model poorly predicted the SOWFA power output results of the turbines farther downstream. Again, a modification of k_e is suggested to address this discrepancy. Specifically, the value of k_e fit to the wake of the upstream turbine is related to the process of making a wake from the freestream. The wake of the second turbine should be adjusted, because its inflow is already

Table II. Causal relations in the two-turbine setup. Red arrows highlight conflicting impacts on wind velocity at the downstream turbine.

Induction	Near-wake velocity	Induced turbulence	Mixing	Recovery	Wake velocity at next turbine
↓	↑	↓	↓	↓	≈
↑	↓	↑	↑	↑	≈

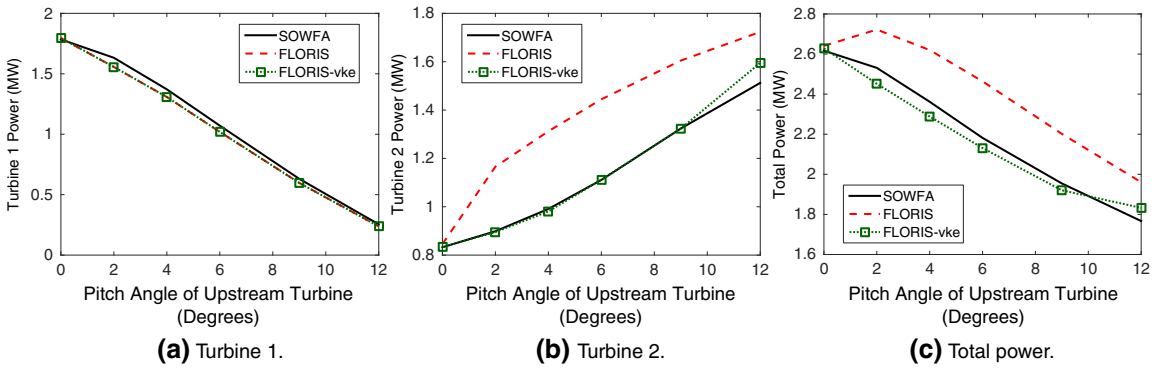

Figure 11. Comparison of the SOWFA, FLORIS and FLORIS-vk$_e$ predictions for the two-turbine scenario.

Wind Energ. 2016; **19**:1135–1150 © 2015 John Wiley & Sons, Ltd.
DOI: 10.1002/we

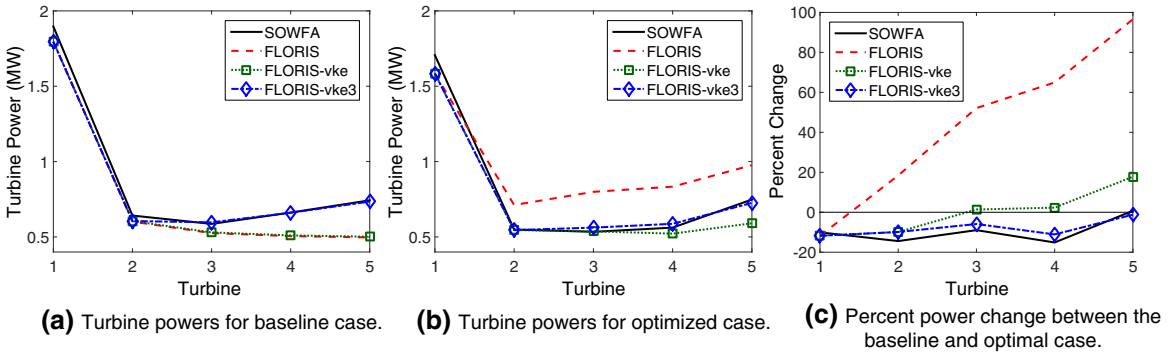

(a) Turbine powers for baseline case. **(b)** Turbine powers for optimized case. **(c)** Percent power change between the baseline and optimal case.

Figure 12. A comparison of results of FLORIS, FLORIS-vk$_e$, FLORIS-vk$_e$3 and SOWFA, for the five-turbine case using baseline axial-induction settings and axial-induction settings that were optimized using the Jensen model.

Table III. FLORIS-vk$_e$3 parameters.

m	b	c
0.1995	−0.0011	0.008276

waked, and the second turbine adds more turbulence. This adjustment should be compounded somewhat at the third turbine, because it is in two wakes, suggesting a summation of effects.

An additional modification is proposed to capture this effect. A wake adjustment term for k_e is introduced for each turbine, based on the axial-induction setting of the turbines that are waking it. Combining this with the adjustment for the axial induction of the turbine itself, as introduced in FLORIS-vk$_e$, yields the following k_e value for a turbine j:

$$k_e(j) = b + ma_j + c \sum_{i:A_{i,j}^{\text{overlap}} \neq 0} \frac{a_i}{a_{\max}} \tag{13}$$

where c is a new fitting parameter, $a_{\max} = \frac{1}{3}$ is introduced for normalization and $A_{i,j}^{\text{overlap}}$ is the overlap area of the wake of an upstream turbine i with the rotor of turbine j. In the aforementioned formulation, a higher k_e results if the rotor is overlapped by other wakes. For the front-most turbine in a row of turbines, the newly introduced adjustment term is zero.

Incorporating the aforementioned formulation gives the further modified model FLORIS-vk$_e$3 (in which the 3 indicates the three free parameters). The newly introduced gain factor, c, was fit to the baseline SOWFA five-turbine scenario assuming the values of m and b are determined from the two-turbine scenarios. This yielded the values shown in Table III.

The five-turbine scenarios were compared across the models, as shown in Figure 12. Figure 12(a) shows that the FLORIS-vk$_e$3 modification significantly improves the consistency to the baseline SOWFA results on the most-waked turbines farther downstream. Figure 12(b) and (c) shows that this improvement extended to the optimized scenario.

As a final analysis of the ability of the FLORIS-vk$_e$3 model to predict the combined effect of pitch and wake overlap, we simulated the five-turbine case in SOWFA with a range of pitch settings on the front turbine. In each case, the pitch setting on the back four turbines was kept at zero. Also, in these cases, the average total power production could not be improved by using the pitch offsets according to both SOWFA and FLORIS-vk$_e$3. In each case, FLORIS-vk$_e$3 was able to best predict the pitch effect on the average power of the downstream turbines in SOWFA, except for Turbine 4 in the case of a 1-degree pitch offset on Turbine 1, see Figure 13. It should be noted that in that case, the SOWFA-predicted power was averaged over a shorter time period (from 1,000 to 1,200 s instead of 1,000 to 2,000 s after the start of the simulation) because of limits on the computational resources. This allowed for higher variance in the SOWFA result for a 1-degree pitch offset. In each pitch-offset case, the FLORIS-vk$_e$3 model extension was shown to be needed to predict the increase in power on the turbines farther downstream when compared with the second and third turbines in the row. This increase can be explained by a fast recovery of the wakes because of increased turbulence intensity.

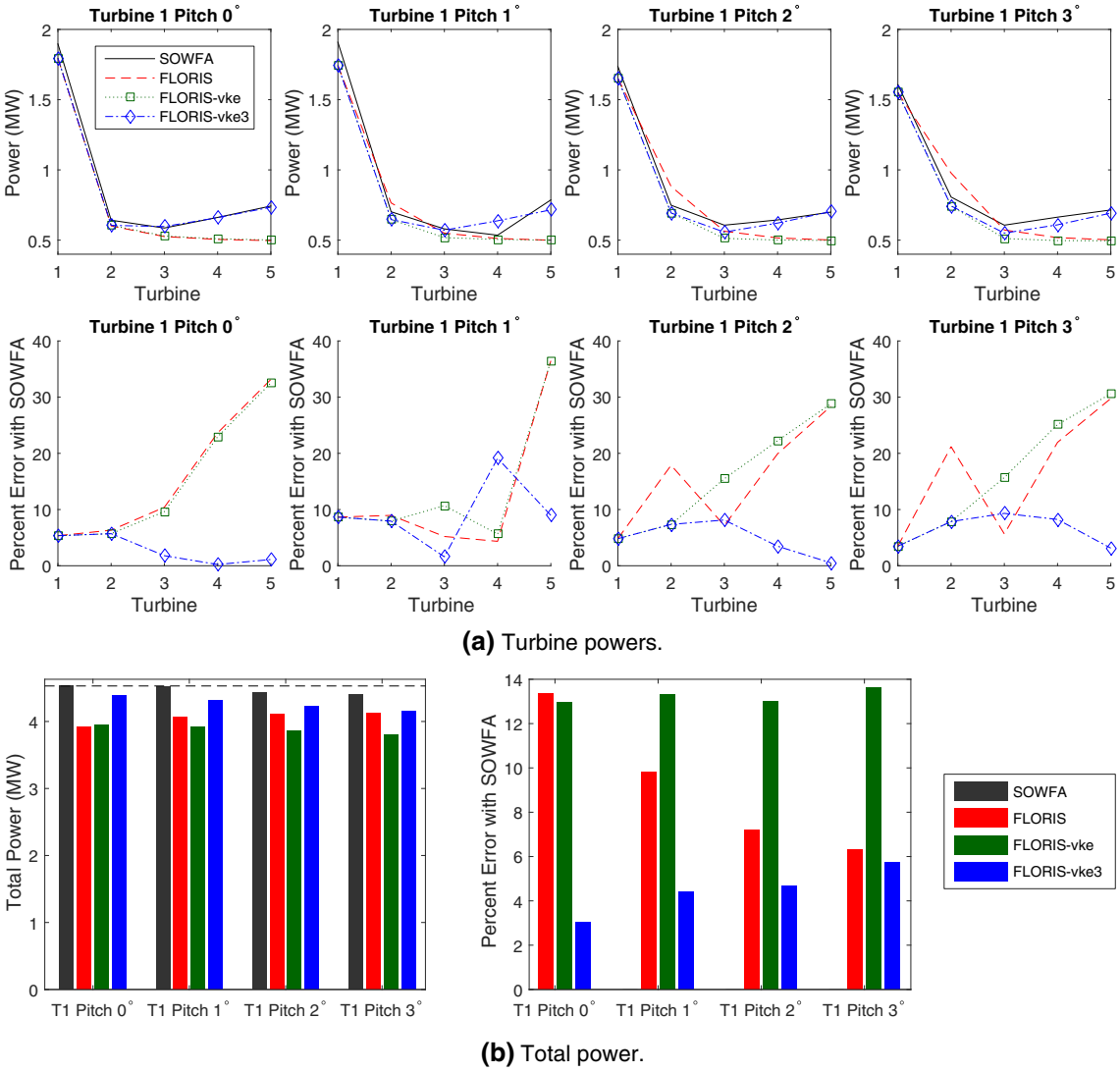

Figure 13. A comparison of the FLORIS, FLORIS-vk$_e$, FLORIS-vk$_e$3 to SOWFA results for a five-turbine case, for a range of pitch settings on the front turbine.

7. CONCLUSION

The potential gain from plant-wide instead of turbine-level optimized axial-induction control, and the particular control settings that yield this gain, depend on the particular atmospheric conditions, the wind plant configuration and the turbine characteristics. The high-fidelity SOWFA simulation examples shown in Section 5.1.2 and 5.2 suggest that there are circumstances which the concept of total wind plant power increase through axial-induction control with pitch or torque offsets is infeasible.

Engineering wake models, such as the Jensen model,[26,27] the Frandsen model[34] or the FLORIS model,[6] take into account wake expansion and recovery and turbine efficiency. The particular wake parameters used in these models will affect the predicted power production increase potential and the optimal control settings. To be able to accurately match the results of axial-induction-based control in the high-fidelity CFD model SOWFA, the rate of wake expansion and recovery in the engineering FLORIS model (an extension of the well-known Jensen model) had to be adjusted to the control operating point (pitch offset) of the wind turbine and to the effect of overlap of several wakes in a row of turbines. These adjustments are included in the FLORIS-vk$_e$3 model.

We conclude that for the considered axial-induction-based control concept to be applied, an optimization strategy for the control settings on the turbines is needed that is adaptive to the particular atmospheric circumstances and turbine char-

Wind Energ. 2016; **19**:1135–1150 © 2015 John Wiley & Sons, Ltd.
DOI: 10.1002/we

acteristics. In the work of Gebraad and van Wingerden,[10] such an adaptive approach is presented. When wind plant control is performed using an engineering model, we recommend (based on the results in this paper) adjusting the model-predicted wake expansion and recovery to the turbine control operating point and including adjustments of wake expansion and recovery at turbines farther downstream in a row.

Future studies will address other effects in a wind plant such as turbulence saturation. There is a saturation point in the turbulence intensity in a line of wind turbines;[35] therefore, the wake adjustment term introduced in equation (13) should presumably remain constant after four to five turbines. Further, FLORIS-vk_e3 was tested only in the case in which all the wakes are fully overlapping. A study of the effect of partial overlap on wake properties is an ongoing work. The additions introduced in FLORIS-vk_e3 will be included in the dynamic extension of FLORIS called FLORIDyn.[36]

In the work of Gebraad *et al.*,[37] the SOWFA results on axial-induction-based wake control are compared with those of yaw-based wake redirection control. Further investigation will consider whether an approach as introduced in the work of Goit and Meyers,[15] in which the axial induction is adapted continuously, has a better potential than the concept with constant offsets that was considered in this paper.

ACKNOWLEDGEMENTS

This work was supported by the U.S. Department of Energy under Contract No. DE-AC36-08GO28308 with the National Renewable Energy Laboratory. Funding for the work was provided by the DOE Office of Energy Efficiency and Renewable Energy, Wind and Water Power Technologies Office. In addition, this work was supported by the National Science Foundation under Grant No. NSF-CMMI-1254129 entitled CAREER: Probabilistic Tools for High Reliability Monitoring and Control of Wind Farms. Any opinions, findings and conclusions or recommendations expressed in this material are those of the authors and do not necessarily reflect the views of the NSF.

The authors thank Matthew Churchfield for his help discussing ideas regarding axial-induction-based control and running simulations in SOWFA.

Delft University of Technology's contributions were supported by the Far Large Offshore Wind (FLOW) project no. 201101 'Offshore wind power plant control for minimal loading' and by the NWO Veni Grant no. 11930 'Reconfigurable floating wind plant'.

REFERENCES

1. Dahlberg J, Medici D. Potential improvement of wind turbine array efficiency by active wake control. *European Wind Energy Conference*, Madrid, Spain, 2003; 65–84.
2. Adaramola MS, Krogstad PÅ. Experimental investigation of wake effects on wind turbine performance. *Renewable Energy* 2011; **36**(8): 2078–2086.
3. Jiménez A, Crespo A, Migoya E. Application of a LES technique to characterize the wake deflection of a wind turbine in yaw. *Wind Energy* 2010; **13**: 559–572.
4. Fleming PA, Gebraad PMO, Lee S, van Wingerden JW, Johnson K, Churchfield M, Michalakes J, Spalart P, Moriarty P. Evaluating techniques for redirecting turbine wakes using SOWFA. *Renewable Energy* 2014; **70**: 211–218.
5. Fleming P, Gebraad PMO, Lee S, van Wingerden JW, Johnson K, Churchfield M, Michalakes J, Spalart P, Moriarty P. Simulation comparison of wake mitigation control strategies for a two-turbine case. *Wind Energy* 2014.
6. Gebraad PMO, Teeuwisse FW, van Wingerden JW, Fleming PA, Ruben SD, Marden JR, Pao LY. Wind plant power optimization through yaw control using a parametric model for wake effects—A CFD simulation study. *Wind Energy* 2014.
7. Horvat T, Spudic V, Baotic M. Quasi-stationary optimal control for wind farm with closely spaced turbines. *MIPRO International Convention*, Opatija, Croatia, 2012; 829–834.
8. Johnson K, Fritsch G. Assessment of extremum seeking control for wind farm energy production. *Wind Engineering* 2012; **36**: 701–716.
9. Marden JR, Ruben SD, Pao LY. A model-free approach to wind farm control using game theoretic methods. *IEEE Transactions on Control Systems Technology* 2013; **21**: 1207–1214.
10. Gebraad PMO, van Wingerden JW. Maximum power-point tracking control for wind farms. *Wind Energy* 2014; **14**: 877–894.
11. Heer F, Esfahani PM, Kamgarpour M, Lygeros J. Model based power optimisation of wind farms. *European Control Conference*, Strasbourg, France, 2014; 1145–1150.

12. Soleimanzadeh M, Wisniewski R, Johnson K. A distributed optimization framework for wind farms. *Journal of Wind Engineering and Industrial Aerodynamics* 2013; **123**: 88–98.
13. Schepers JG, Van der Pijl SP. Improved modelling of wake aerodynamics and assessment of new farm control strategies. *Journal of Physics: Conference Series,* IOP Publishing 2007; **75**(1).
14. Annoni J, Seiler P, Johnson K, Fleming P, Gebraad P. Evaluating wake models for wind farm control. *American Control Conference*, Portland, OR, USA, 2014; 2517–2523.
15. Goit JP, Meyers J. Optimal control of energy extraction in wind-farm boundary layers. *Journal of Fluid Mechanics* 2015; **768**: 5–55.
16. Nilsson K, Ivanell S, Hansen KS, Mikkelsen R, Sørensen JN, Breton SP, Henningson Dan. Large-eddy simulations of the Lillgrund wind farm. *Wind Energy* 2014; **18**: 449–467.
17. Knudsen T, Bak T, Svenstrup M. Survey of wind farm control—power and fatigue optimization. *Wind Energy* 2014.
18. Boorsma K, Heat and flux. Analysis of field measurements. *Technical Report ECN-E–12-048*, Energy Research Centre of the Netherlands, Petten, Netherlands, 2012.
19. Bianchi FD, Battista HD, Mantz RJ. *Wind Turbine Control Systems; Principles, Modelling and Gain Scheduling Design*. Springer-Verlag: London, UK, 2007.
20. Jonkman J, Butterfield S, Musial W, Scott G. Definition of a 5-MW reference wind turbine for offshore system development. *Technical Report NREL/TP-500-38060*, National Renewable Energy Laboratory, Golden, Colorado, USA, 2009.
21. España G, Aubrun S, Loyer S, Devinant P. Spatial study of the wake meandering using modelled wind turbines in a wind tunnel. *Wind Energy* 2011; **14**: 923–937.
22. Larsen GC, Madsen HA, Thomsen K, Larsen TJ. Wake meandering: a pragmatic approach. *Wind Energy* 2008; **11**(4): 377–395.
23. Medici D, Alfredsson PH. Measurements on a wind turbine wake: 3D effects and bluff body vortex shedding. *Wind Energy* 2006; **9**: 219–236.
24. Abkar M. The effect of atmospheric stability on wind-turbine wakes: A large-eddy simulation study. *Journal of Physics: Conference Series,* IOP Publishing 2014; **524**(1).
25. Barthelmie RJ, Jensen LE. Evaluation of wind farm efficiency and wind turbine wakes at the Nysted offshore wind farm. *Wind Energy* 2010; **13**: 573–586.
26. Jensen NO. A note on wind generator interaction. *Technical Report Risø-M-2411*, Risø National Laboratory, Roskilde, Denmark, 1984.
27. Katić I, Højstrup J, Jensen NO. A simple model for cluster efficiency. *EWEA Conference and Exhibition*, Rome, Italy, 1986; 407–410.
28. Churchfield M, Lee S. NWTC information portal (SOWFA), 2014. Available: https://nwtc.nrel.gov/SOWFA [Accessed on July 2014].
29. Jonkman J. NWTC information portal (FAST), 2014. Available: https://nwtc.nrel.gov/FAST [Accessed on July 2014].
30. Churchfield MJ, Lee S, Michalakes J, Moriarty PJ. A numerical study of the effects of atmospheric and wake turbulence on wind turbine dynamics. *Journal of Turbulence* 2012; **13**.
31. National Renewable Energy Laboratory. NREL's high-performance computing capabilities, 2014. Available: http://hpc.nrel.gov [Accessed on July 2014].
32. Churchfield M, Lee S, Moriarty P, Martinez L, Leonardi S, Vijayakumar G, Brasseur J. A large-eddy simulation of wind-plant aerodynamics. *Proceedings of the AIAA Aerospace Sciences Meeting*, Nashville, Tennessee, USA, 2012.
33. Johnson KE, Thomas N. Wind farm control: addressing the aerodynamic interaction among wind turbines. *American Control Conference*, St. Louis, USA, 2009; 2104–2109.
34. Frandsen S, Barthelmie R, Pryor S, Rathmann O, Larsen S, Højstrup J, Thøgersen M. Analytical modelling of wind speed deficit in large offshore wind farms. *Wind Energy* 2006; **9**(1-2): 39–53.
35. Chamorro LP, Porté-Agel F. Turbulent flow inside and above a wind farm: a wind-tunnel study. *Energies* 2011; **4**: 1916–1936.
36. Gebraad PMO, Van Wingerden JW. A control-oriented dynamic model for wakes in wind plants. *Journal of Physics: Conference Series,* IOP Publishing 2014; **524**(1).
37. Gebraad PMO, Fleming PA, van Wingerden JW. Comparison of actuation methods for wake control in wind plants. *American Control Conference*, Chicago, USA, 2015.

Wind Energ. 2016; **19**:1135–1150 © 2015 John Wiley & Sons, Ltd.
DOI: 10.1002/we